Analysis of Microdischarge Characteristics Induced by Synchronized Auxiliary Address Pulse Based on Cross-Sectional Infrared Observation in AC Plasma Display Panel

Heung-Sik Tae, *Member, IEEE*, Hyun Ju Seo, Dong-Cheol Jeong, Jeoung Hyun Seo, Hyun Kim, and Ki-Woong Whang

***Abstract*—The microdischarge characteristics induced by an auxiliary address pulse with the synchronized application of sustain pulses are investigated based on cross-sectional infrared (IR) (823 nm) observations taken using an image-intensified charge-coupled device (ICCD) camera. The IR observations reveal that the application of an auxiliary short pulse with an optimal amplitude and width to the address electrode enhances the intensity of the IR emission. Furthermore, the cross-sectional IR observations demonstrate that the effective infrared emission region is extended toward the address electrode. In addition, a numerical analysis using a two-dimensional fluid simulation is also applied to investigate the discharge mechanism relative to the amplitude and width of the auxiliary address pulse. As a result, the improvement in the luminance and luminous efficiency was found to be caused by a face discharge between the address and the sustain (or scan) electrodes, where the face discharge plays an important role in supplying priming particles to the surface discharge and lengthening the discharge path, which in turn intensifies the surface discharge.**

***Index Terms*—Auxilliary short pulse, infrared (IR) observations, microdischarge.**

I. Introduction

DESPITE the suitability of flat panel devices for digital high-definition television, the luminous efficiency of plasma display panels (PDPs) is still low. Yet, improving the luminous efficiency of a PDP is very difficult, because the spacing between the PDP cells are too small to produce an efficient discharge. Moreover, in a typical three-electrode PDP structure with coplanar sustain electrodes, the discharge volume is predominantly formed in the vicinity of the surface of the front panel (called a surface discharge), resulting in a small discharge volume and inefficient use of the phosphor layer deposited on the address electrode. Therefore, enlarging the discharge volume toward the address electrode would be expected to improve the discharge efficiency and use of the phosphor layer, thereby improving the luminance and luminous efficiency of the PDP cells with a small spacing. As such, the current authors previously reported that the synchronized application of an auxiliary short pulse to the address electrode during the sustain period did have an impact on improving the luminance and luminous efficiency in an alternating current plasma display panel (ac-PDP) [1], [2]. Recently, several research results on the analysis of the changes in the micro-discharge characteristics according to the application of various auxiliary address pulses have been reported based on direct measurement of the microdischarge volume [3], [4]. However, direct observation of the microdischarge phenomena, particularly a cross-sectional view, with respect to the use of a synchronized auxiliary pulse is still needed to gain a better understanding of the fundamental discharge physics to improve the luminance and luminous efficiency of the microdischarge cells.

Accordingly, in this paper, the microdischarge characteristics induced by applying an auxiliary address pulse with the synchronized application of the sustain pulse during the sustain period were investigated based on cross-sectional (IR) (823 nm) observations taken using an image-intensified charge-coupled device (ICCD) camera. In particular, the effects of the amplitude and width of the auxiliary address pulse on the microdischarge characteristics were examined in detail. In addition, a numerical analysis using a two-dimensional (2-D) fluid simulation is also applied to examine the mechanism of the improved luminance and luminous efficiency caused by the application of a synchronized auxiliary address pulse during the sustain period.

II. Cross-Sectional Infrared Observation Using ICCD Camera

A. Experimental Setup

Fig. 1 shows a schematic diagram of the experimental setup employed in this study. The measurement system mainly consisted of an ICCD camera (ICCD-576EM, Princeton Instrument, Inc.), discharge chambers, manipulator, and driving circuits. The test panel was fabricated to enable the discharge phenomena to be observed from a cross-sectional view of the test cell, and the specifications are given in Table I. The gas mixture Ne–Xe (4%) was filled at a pressure of 300 torr in the discharge chamber. The MgF_2 window was located between

Manuscript received April 26, 2004; revised December 27, 2004. This work was supported by the Brain Korea 21.

H.-S. Tae, H. J. Seo, and H. Kim are with the School of Electronic and Electrical Engineering, Kyungpook National University, Daegu 702-701, Korea (e-mail: hstae@ee.knu.ac.kr).

D.-C. Jeong and K.-W. Whang are with the School of Electrical and Computer Engineering, Seoul National University, Seoul 151-742, Korea.

J. H. Seo is with the Department of Electronics, Incheon University, Incheon 402-749, Korea.

Digital Object Identifier 10.1109/TPS.2005.845065

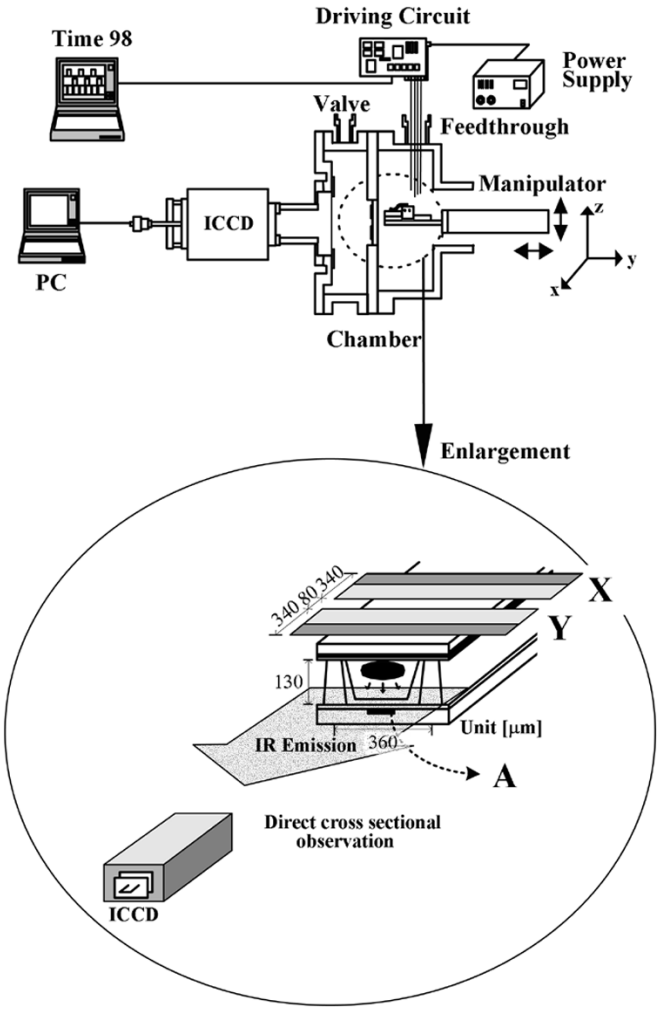

Fig. 1. Schematic diagram of experimental setup for cross-sectional infrared observation using ICCD camera.

TABLE I
SPECIFICATION OF TEST PANEL

Front panel		Rear panel	
ITO width	340μm	Address electrode width	150μm
ITO gap	80μm	Barrier rib height	130μm
Bus width	120μm	Barrier rib pitch	420μm
Dielectric thickness	30μm	Barrier rib width	80μm

the vacuum chamber connected to the ICCD camera and the discharge chamber where the test panel was inserted. An optical filter with a center wavelength of 821 nm and full-width half-maximum (FWHM) of approximately 10 nm was used to measure the IR (823 nm) emission images emitted from the cross-sectional view of the test panel. To measure the time-averaged IR emission images and temporal behavior of the IR emission images, the shutter mode and gate mode of the ICCD camera were used, respectively, where the shutter mode means that the IR emission is superposed during an exposure time of 20 ms, while the gate mode means that the IR emission is superposed during an exposure time of 20 ns, thereby providing information on the time behavior of the IR emission from the test cell relative to a variation in the auxiliary address pulse.

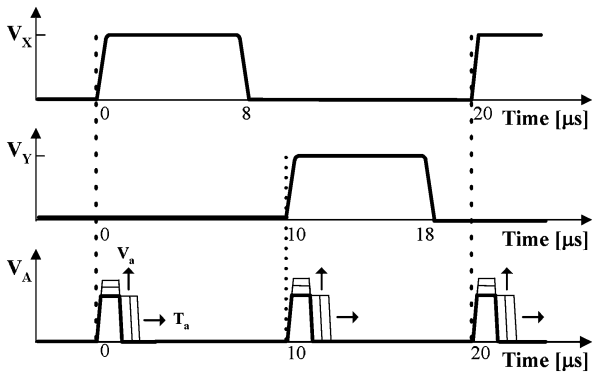

Fig. 2. Driving waveforms for applying synchronized auxiliary address pulse.

Fig. 2 shows the driving waveforms V_X, V_Y, and V_A applied to the sustain electrodes X, and Y, and address electrode A, respectively, where V_A is the auxiliary pulse applied synchronously with the application of the sustain pulses V_X and V_Y. The driving conditions were a sustain frequency of 50 kHz with a 40% duty ratio and amplitude of 180 V. The amplitudes of the auxiliary pulses (V_a) were varied at intervals of 30 V from 0 V to 150 V, whereas the widths of the auxiliary pulses (T_a) were varied at intervals of 200 ns from 400 ns to 1 μs.

B. Cross-Sectional IR Observation Relative to Amplitude and Width of Auxiliary Address Short Pulse

Fig. 3 illustrates the time-averaged IR emission images measured from the cross-sectional view of the test cell using the shutter mode of the ICCD camera when the amplitudes of the auxiliary address pulses were varied at intervals of 30 V from 0 to 120 V at a constant width of 400 ns. The blur in the images in Fig. 3 was due to the amplification of the light emission from the cell, plus the color bar shown below the IR images indicates the intensity of the IR emission. As shown in Fig. 3, with an increase in the amplitude of the address pulse from 0 until 90 V, the IR emission intensity increased, plus the distribution area of the intensive IR emission also extended toward the address electrode. Conversely, at an address voltage higher than 90 V, both the IR emission intensity and the distribution area tended to decrease.

Fig. 4 illustrates the temporal behavior of the IR emission images measured from the cross-sectional view of the test cell using the gate mode of the ICCD camera when the amplitudes of the auxiliary address pulses were varied at intervals of 30 V from 0 to 120 V at a constant width of 400 ns. In the conventional case $(V_a = 0\ \mathrm{V})$, the maximum peak intensity of the IR emission was observed at 400 ns after the application of the sustain pulse. Meanwhile, in the case of applying an auxiliary address pulse of 30 V, both the maximum value and the time behavior of the IR emission intensity were almost the same as those in the conventional case, indicating that the sustain discharge was unaffected by the application of a low address voltage. However, the application of an auxiliary address pulse greater than 60 V induced a faster discharge initiation, and also extended the intensified IR emission region toward the address electrode. Furthermore, with an auxiliary address pulse of 90 V, a very fast discharge was ignited and the maximum value of the IR

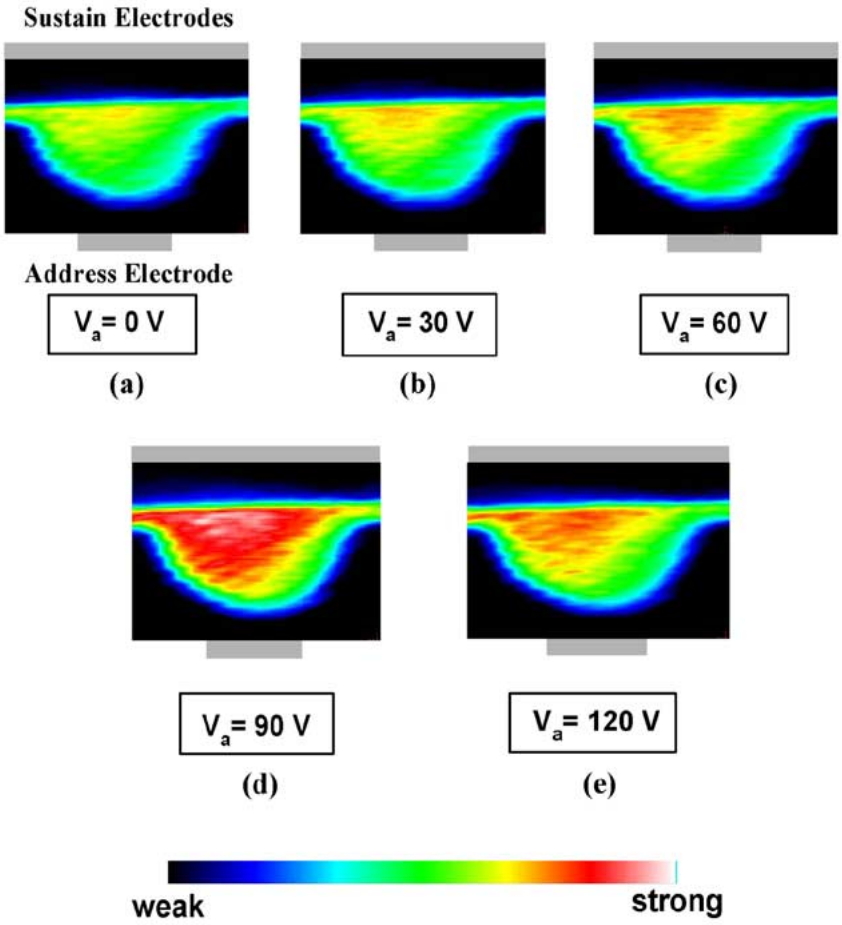

Fig. 3. Cross-sectional view of time-averaged IR emission images using shutter mode of ICCD camera when amplitude of auxiliary address pulse was varied at intervals of 30 V from 0 to 120 V at constant width of 400 ns.

emission intensity was observed at 240 ns. In this case, the fast discharge initiation can be explained as follows [5]. Unlike the conventional sustain discharge $(V_a = 0\ \mathrm{V})$, the synchronized application of an auxiliary address pulse with an appropriately high amplitude and short width effectively initiated a face discharge between the address and sustain electrodes prior to the main sustain surface discharge between the two sustain electrodes. Moreover, this fast discharge initiation caused by the application of the auxiliary address pulse provided priming particles for a more efficient main surface discharge between the sustain electrodes. Consequently, as shown in Fig. 4(d), the discharge efficiency was enhanced, plus the discharge volume with the intensive IR emission was also extended toward the address electrode by means of the synchronized application of the auxiliary address pulse with an appropriately high amplitude and short width. In contrast, with an auxiliary address pulse of 120 V, both the IR emission intensity and the distribution area tended to decrease, indicating that the application of too high an address voltage disturbed the main sustain discharge. The detailed mechanism will be described in Section III using a 2-D fluid simulation.

Figs. 5 and 6 illustrate the time-averaged image and temporal behavior of the IR emission measured from a cross-sectional of the test cell using the shutter (Fig. 5) and gate (Fig. 6) modes of the ICCD camera when the widths of the auxiliary address pulses were varied at intervals of 200 ns from 0 ns to 1 μs at a constant amplitude of 90 V. The results in Figs. 5 and 6 show that as the pulse width of the auxiliary address pulse was shortened, the corresponding IR emission intensity was enhanced and its distribution further extended toward the address electrode. As such, this means that the use of an auxiliary address pulse was most efficient at the initiation of the sustain discharge, and less efficient during the sustain discharge, since it may have disturbed the accumulation of wall charges on the sustain electrodes for a stable subsequent sustain discharge. As seen in Figs. 5 and 6, an address pulse of 90 V with a width of 400 ns produced the highest IR intensity with the largest distribution area toward the address electrode. The detailed mechanism will also be described in Section III using a 2-D fluid simulation.

III. Numerical Analysis

To investigate the effect of an auxiliary address pulse during the sustain period, a numerical analysis using a 2-D fluid model was applied [6], including Poisson, continuity, and drift-diffusion equations [7]. It was assumed that the local field approximation, i.e., the ionization and excitation rates, were functions of the local field [8]. The reaction model consisted of 8 levels for Xe and six levels for Ne, and the secondary electron coefficient (γ) was assumed to be 0.2 for the Ne ions and 0.02 for

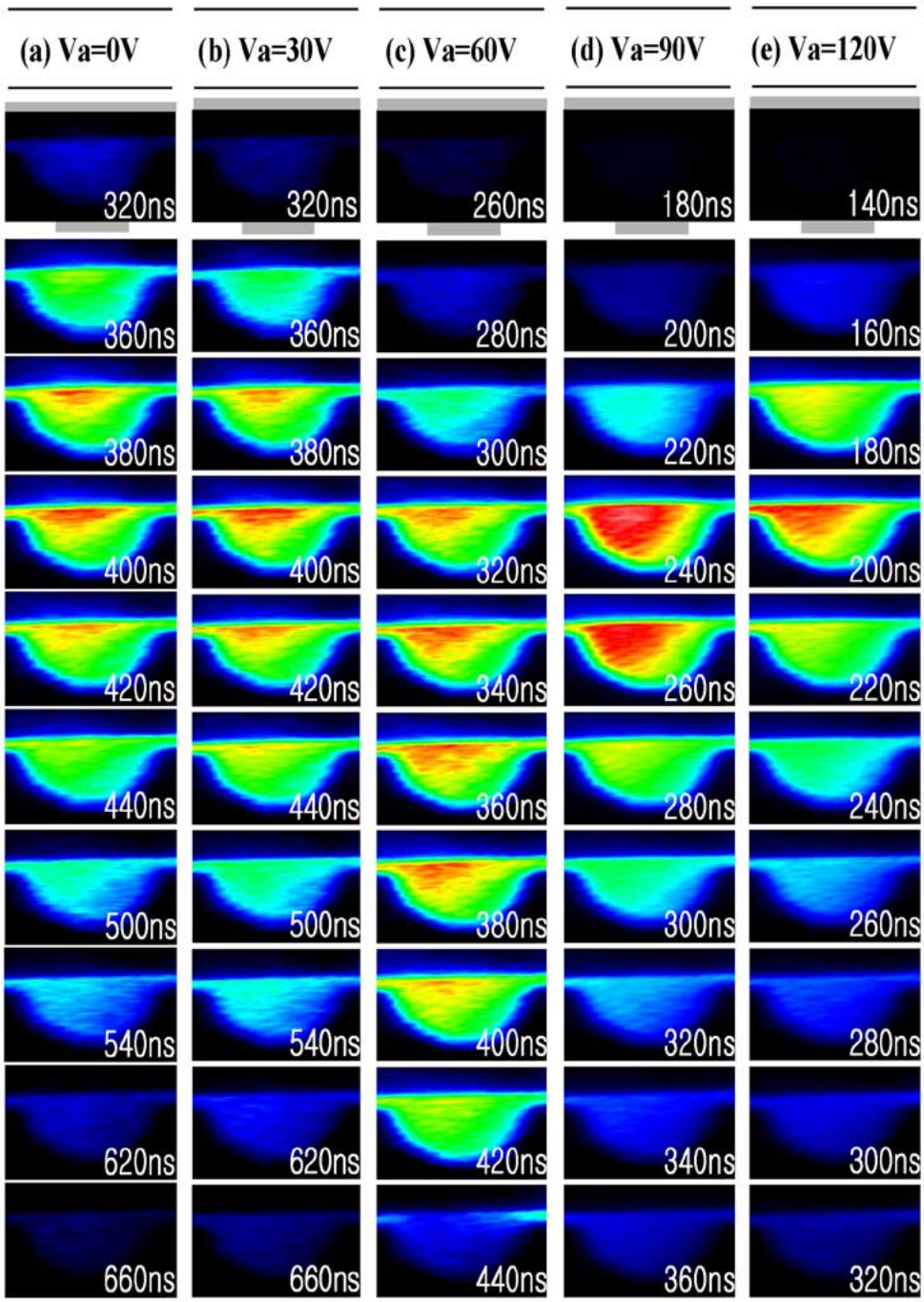

Fig. 4. Cross-sectional view of temporal behavior of IR emission images using gate mode of ICCD camera when amplitude of auxiliary address pulse was varied at intervals of 30 V from 0 to 120 V at constant width of 400 ns.

the Xe ions. The cell used in this model was a conventional surface type ac PDP. Fig. 7 shows the computational area and cell specifications.

In the simulation, the address pulse width (T_a) was varied from 0.2 to 0.5 μs, which was slightly different from the experimental conditions. According to the experiment, the address pulse had a significant effect on the sustain discharge when the pulse was varied during the sustaining discharge. However, in the 2-D simulation, since the charge loss to the barrier rib could not be considered, the discharge was more easily ignited than in the real situation, resulting in a faster discharge ignition and termination. Therefore, the address pulse width and rising time were adjusted to make them suitable for the simulation.

To compare the simulation results with the experimental results, the physical parameters of the luminance and luminous efficiency were defined as simulation terms, where the luminance was inferred from the amount of vacuum ultraviolet (VUV) generation, while the luminous efficiency was inferred from the VUV generation efficiency. Plus, since the VUV generation efficiency (ρ_{VUV}) is proportional to the Xe excitation efficiency (ρ_{exi}), as the VUV radiation comes from the Xe excited state, the Xe excitation efficiency was divided into two partial effi-

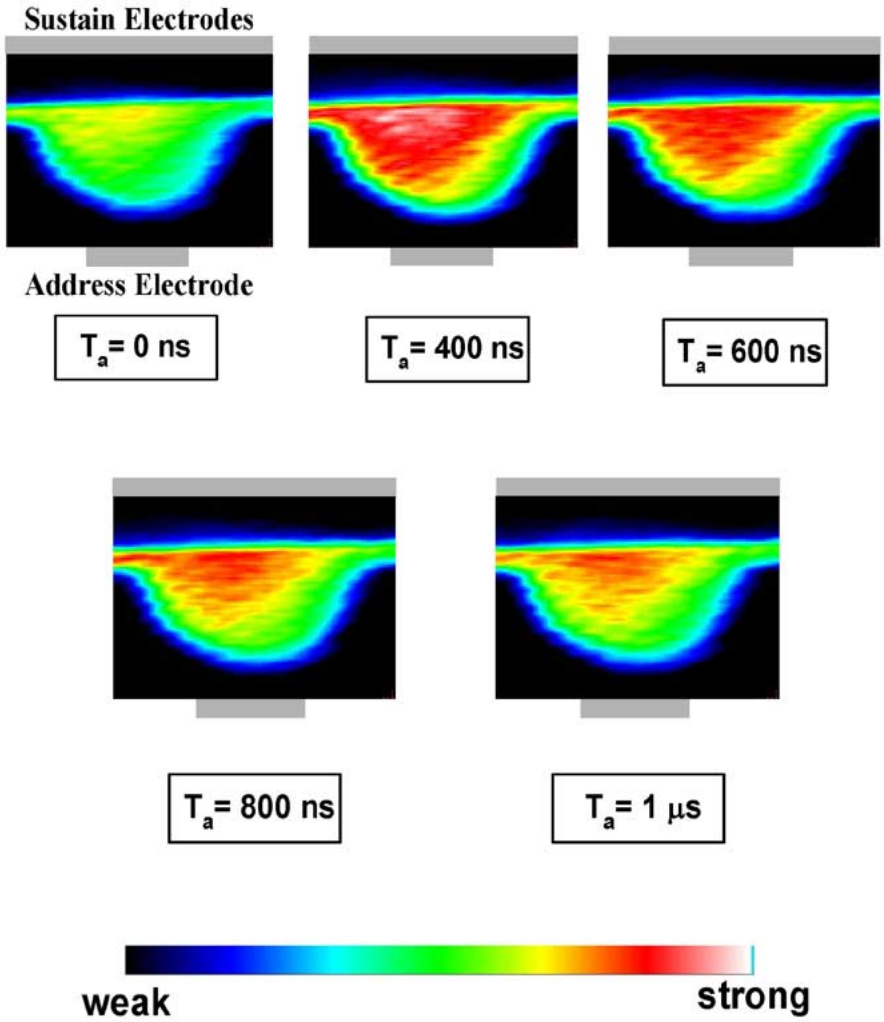

Fig. 5. Cross-sectional view of time-averaged IR emission images using shutter mode of ICCD camera when width of auxiliary address pulse was varied at intervals of 200 ns from 0 ns to 1 μs at constant amplitude of 90 V.

ciencies: the electron heating efficiency (ρ_1) by an electric field and the Xe excitation efficiency (ρ_2) by electrons. The definition and relation of the partial efficiencies are shown by the following equation:

$$\rho_{\mathrm{VUV}} \propto \rho_{\mathrm{exi}} = \frac{W_{\mathrm{exi}}}{W_{\mathrm{tot}}} = \frac{W_{\mathrm{ele}}}{W_{\mathrm{tot}}} \times \frac{W_{\mathrm{exi}}}{W_{\mathrm{ele}}} = \rho_1 \times \rho_2$$

where W_{tot} is the total electric power input, W_{ele} is the electric power delivered to the electrons, and W_{exi} is the power consumed for Xe excitation. Plus, ρ_1 is mainly determined by the density ratio of electrons to ions in the discharge space and also affected by the transient spatial field, while ρ_2 is mainly determined by the electron temperature.

Fig. 8 shows the luminance and luminous efficiency as a function of the bias voltage on the address electrode when T_a is 0.2 μs. The luminance increased by about 60% and showed a peak value around $V_a = 60 \sim 70$ V, plus the luminous efficiency was also significantly improved by about 25%. Accordingly, the simulation results showed a good agreement with the experimental results, even though the exact values for the two cases were somewhat different.

Figs. 9 and 10 show the current flows and transient excitation efficiencies for $V_a = 10$ and 70 V, respectively. The main difference in $\rho_{\mathrm{exi}}(t)$ between $V_a = 10$ and 70 V was the initial step during the discharge, plus in the case of $V_a = 10$ V, $\rho_{\mathrm{exi}}(t)$ had the highest value in the decreasing current region where the main discharge terminated. Conversely, as shown in Fig. 10(b), $\rho_{\mathrm{exi}}(t)$ at $V_a = 70$ V showed an abrupt increase at the initial discharge and maintained a high efficiency during the discharge. In Figs. 9(b) and 10(b), although the value of $\rho_{\mathrm{exi}}(t)$ was high after the discharge termination, this was irrelevant, as it had no affect on the luminance and luminous efficiency.

The main difference in the current flows between the two cases was related to the address current. As shown in Fig. 9(a), a positive current (i.e., ions) flowed through the address electrode, while in Fig. 10(a), a negative current (i.e., electrons) flowed during the time when the address pulse was On and a positive current (i.e., ions) flowed toward the address electrode after the address pulse was Off. Fig. 10(a) reveals that a discharge was initiated between the address and Y electrodes (hereafter face discharge) prior to the X–Y discharge, thereby confirming that the face discharge was responsible for the improved efficiency.

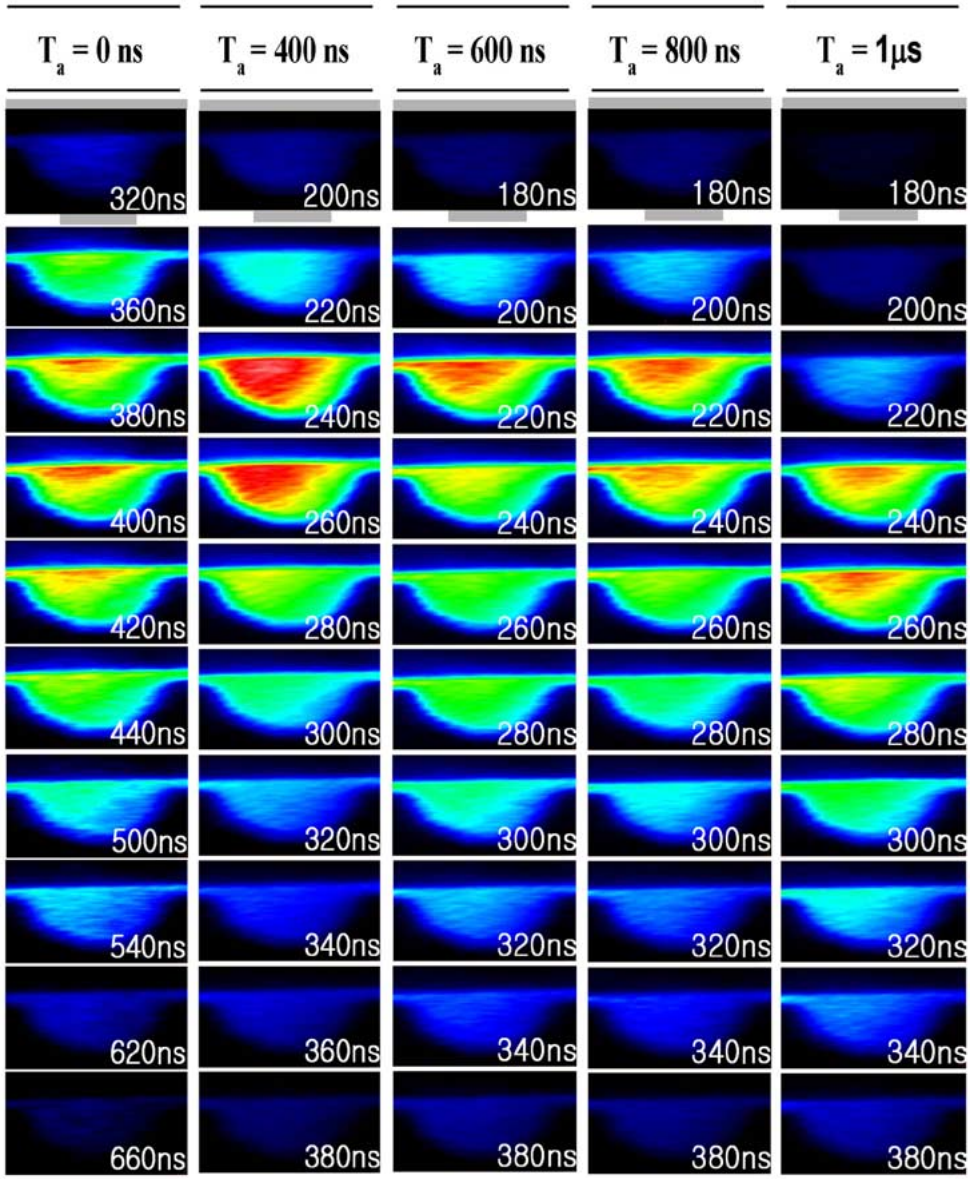

Fig. 6. Cross-sectional view of temporal behavior of IR emission images using gate mode of ICCD camera when width of auxiliary address pulse was varied at intervals of 200 ns from 0 ns to 1 μs at constant amplitude of 90 V.

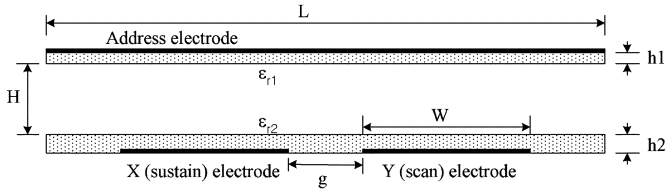

Symbol	Parameter	Value
L	cell pitch	1080μm
H	barrier rib height	130μm
h1	thickness of phosphor layer	10μm
h2	thickness of front dielectric layer	30μm
W	width of sustain electrode	340μm
g	gap between sustain electrodes	80μm
ε_{r1}	relative dielectric constant of phosphor	3
ε_{r2}	relative dielectric constant of dielectric layer	15

Fig. 7. Computational area and cell specifications used in simulation.

To understand this more clearly, the spatiotemporal behavior of the electrons during the discharge is plotted in Figs. 11 and 12 for the two cases, respectively. As shown in Fig. 11(a), two density peaks were observed at $t = 30.1$ μs, where one peak was above the inner edge of the X electrode and the other was below the address electrode. The peak density of electrons above the X electrode was almost three times higher than that below the address electrode, meaning that the discharge between the X and Y electrodes was more intense than that between the address and Y electrodes. Fig. 11(b) shows the density profile at 30.2 μs. As the cathode sheath had not yet been formed, the peak only appeared above the X electrode. Fig. 11(c) shows the electron density distribution when the discharge current flow was at maximum and the electrons were mainly distributed around the gap between the X and Y electrodes.

In contrast, in the case of $V_a = 70$ V, the peak density appeared below the address electrode at 30.1 μs, indicating that the initial discharge was initiated between the address and Y electrodes. With an increase in the sustain voltage (because the

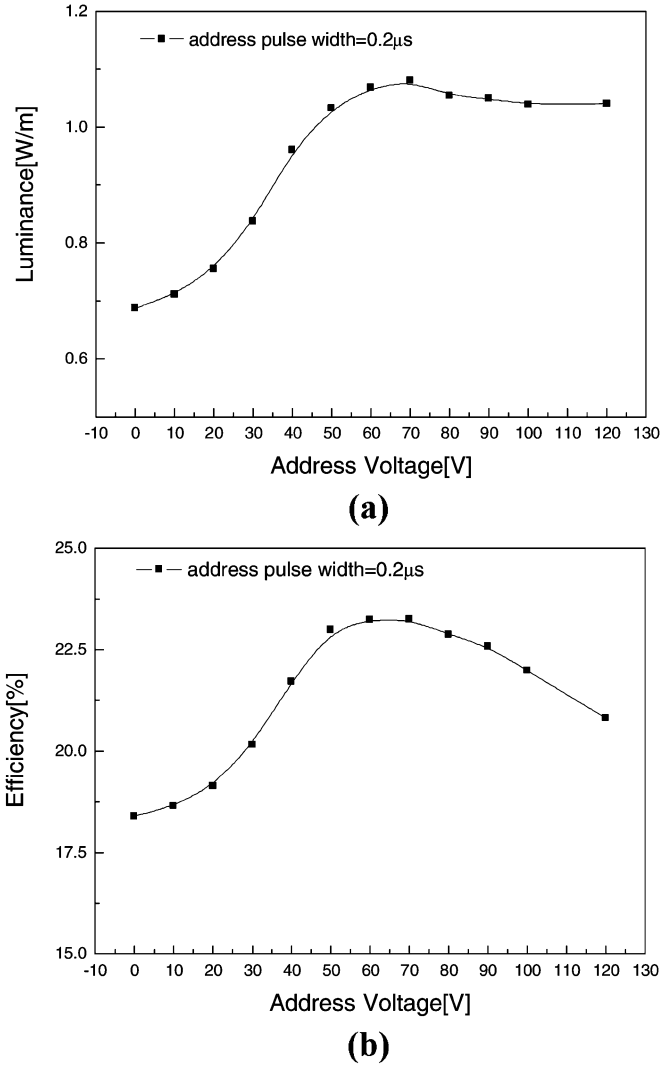

Fig. 8. Luminance and luminous efficiency as function of bias voltage on address electrode when Ta was 0.2 μs.

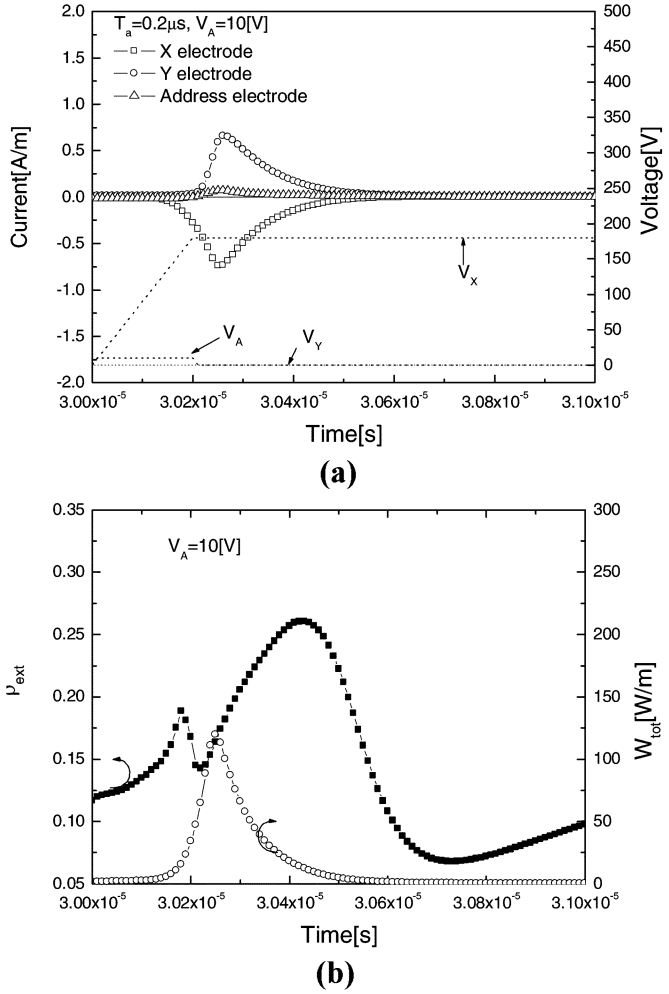

Fig. 9. Current flow and temporal behavior of luminous efficiency at $V_a = 10$ V, $T_a = 0.2$ μs: (a) current flows through three electrodes, and (b) temporal behavior of luminous efficiency.

rising time was 0.2 μs), a discharge started to form between the X and Y electrodes. At this point, the abundant electrons below the address electrode moved toward the X electrode, because the bias of X was higher than that of the address electrode. These electrons then intensified the discharge between the X and Y electrodes, and lengthened the discharge path. Generally, a surface discharge occurs between the inner edges of the X and Y electrodes, as shown in Fig. 11(c), which means the discharge path is very short. However, when a face discharge was ignited before the surface discharge, the electrons generated by the face discharge also took part in the surface discharge. Plus, since these electrons traveled a longer distance, they gained more energy, generating more electrons, ions, and Xe-excited species. As a result, the luminance and luminous efficiency were improved. When the results in Fig. 12(c) were compared with those in Fig. 11(c), the discharge volume in Fig. 12(c) was found to be larger than that in Fig. 11(c).

Until now, only the positive effects of the face discharge have been investigated, however, it can also have some negative effects. Although the face discharge was found to supply priming particles, it also erased some of the wall charges on the Y (or X) electrode. As shown in Fig. 8, when V_a was above 70 V, the luminance and luminous efficiency slightly decreased. Usually, the discharge efficiency tends to be proportional to the length of discharge path. Thus, the face discharge efficiency is less effective than the surface discharge efficiency because a face discharge path is shorter than a surface discharge path. Also, the discharge volume of a face discharge is smaller than that of a surface discharge. Therefore, the luminance and luminous efficiency of the face discharge were not as good as those of the surface discharge. When the address voltage was increased, the face discharge became larger, yet the surface discharge following the face discharge was weakened, because the wall charges on the Y (or X) electrode were decreased with an increase in the address voltage. As such, the luminance and luminous efficiency actually decreased with a high address voltage.

Fig. 13(a) and (b) show the variations in the luminance and luminous efficiency as a function of the address voltage (V_a) ranging from 10 to 120 V at $T_a = 0.2$ μs and address pulse width (T_a) ranging from 0.1 to 1 μs at $V_a = 70$ V, respectively. As mentioned previously, Fig. 13(a) revealed an optimal address voltage condition i.e., 60 V (90 V in the experimental

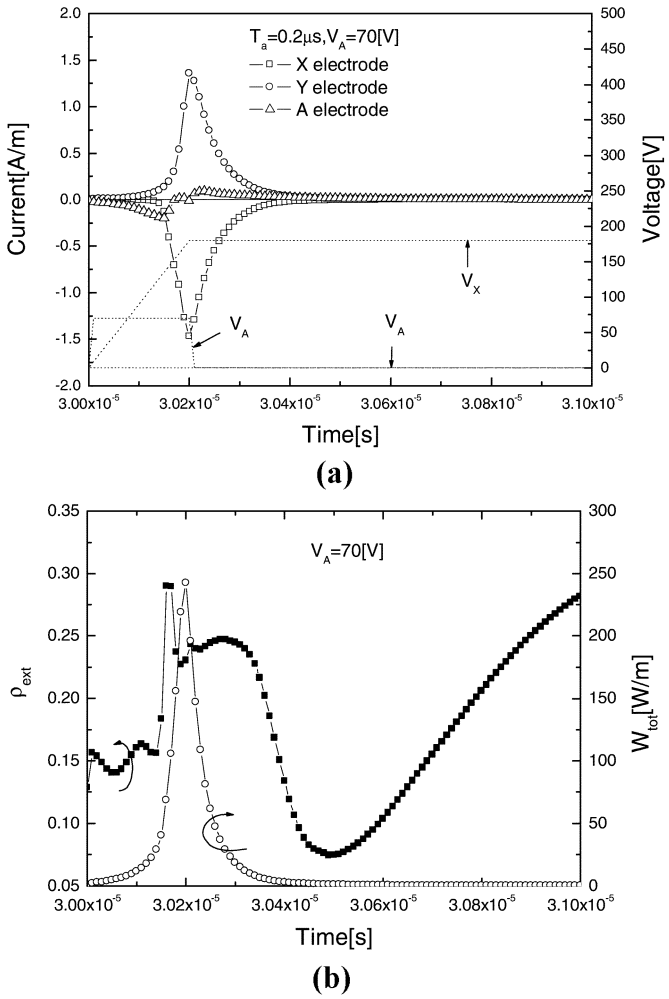

Fig. 10. Current flow and temporal behavior of luminous efficiency at $V_a = 70\,\mathrm{V}, T_a = 0.2\ \mu\mathrm{s}$: (a) current flows through three electrodes, and (b) temporal behavior of luminous efficiency.

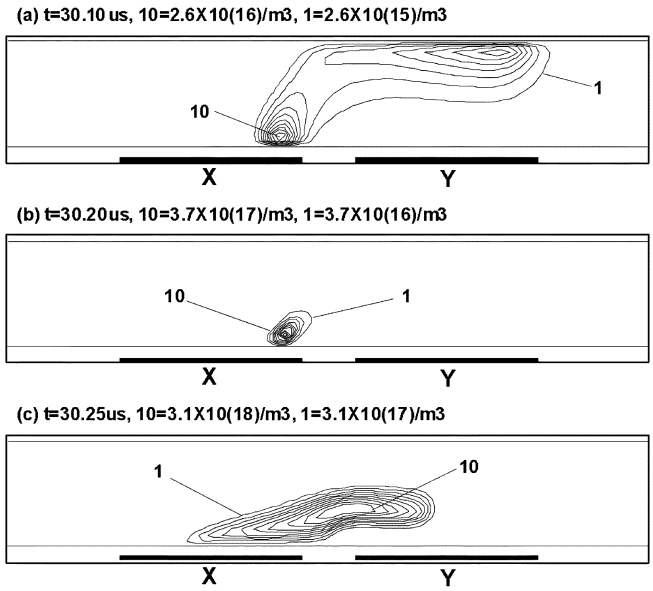

Fig. 11. Spatiotemporal variation of electron density at $V_a = 10\,\mathrm{V}, T_a = 0.2\ \mu\mathrm{s}$.

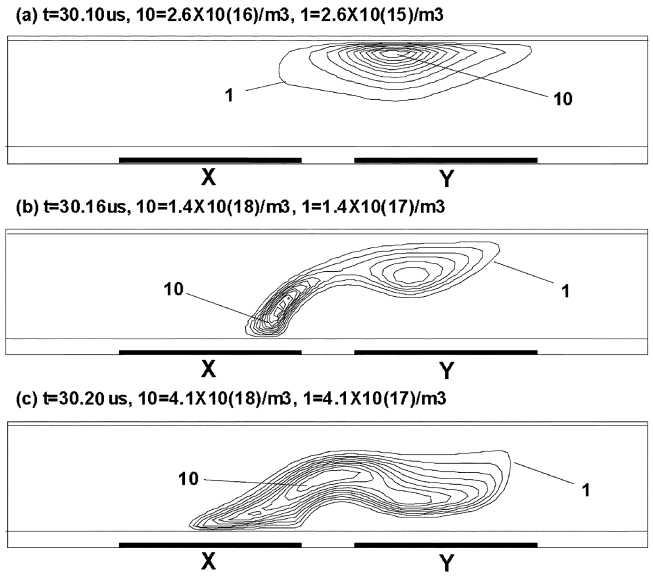

Fig. 12. Spatiotemporal variation of electron density at $V_a = 70\,\mathrm{V}, T_a = 0.2\ \mu\mathrm{s}$.

results). For the address pulse width, as shown in Fig. 13(b), it was obvious that a shorter pulse was more effective, which could also be easily inferred from the existing understanding. To improve the luminous efficiency, a face discharge must be formed for every sustain pulse. However, to ignite a successive face discharge at the next pulse, the wall charges erased from the address electrode by the previous face discharge must be restored. As such, when a shorter pulse width than the width of the surface discharge current flow (hereafter T_{CFA}) was used, the wall charges erased from the address electrode were automatically restored, as shown in Fig. 10(a). After the face discharge occurred, the address pulse became 0 V. The address electrode then acted like a cathode and many ions were accumulated on the address electrode, enabling the face discharge to ignite at the next pulse. However, when T_a was larger than T_{CFA}, the accumulated ion wall charges were insufficient, because the address voltage was high during the surface discharge. As such, a face discharge did not occur at the next sustain pulse.

Although the effects of the address voltage and pulse width have already been discussed, there is still an unanswered question. When the address pulse width was above 0.5 μs, the luminous efficiency was about 5% improved compared with the case of no address pulse. However, the luminance was improved by about 30%. Meanwhile, although an address pulse width above 0.5 μs did not ignite a face discharge, the luminance was still increased about 30% under this condition.

Previous results revealed that when adopting a constant address bias, the plasma shields out a constant address bias, no matter what the address bias is [6]. As such, when the address bias is lower than $V_S/2$, the ions accumulate on the surface of the address electrode. Whereas, when the address bias is higher than $V_S/2$, the electrons accumulate on the surface of the address electrode to shield out the bias effect. Hence, no matter what the address bias is, it does not affect the luminance and luminous efficiency.

The results in Fig. 13 are similar to the condition of a constant address bias, yet with one different aspect. The address bias was

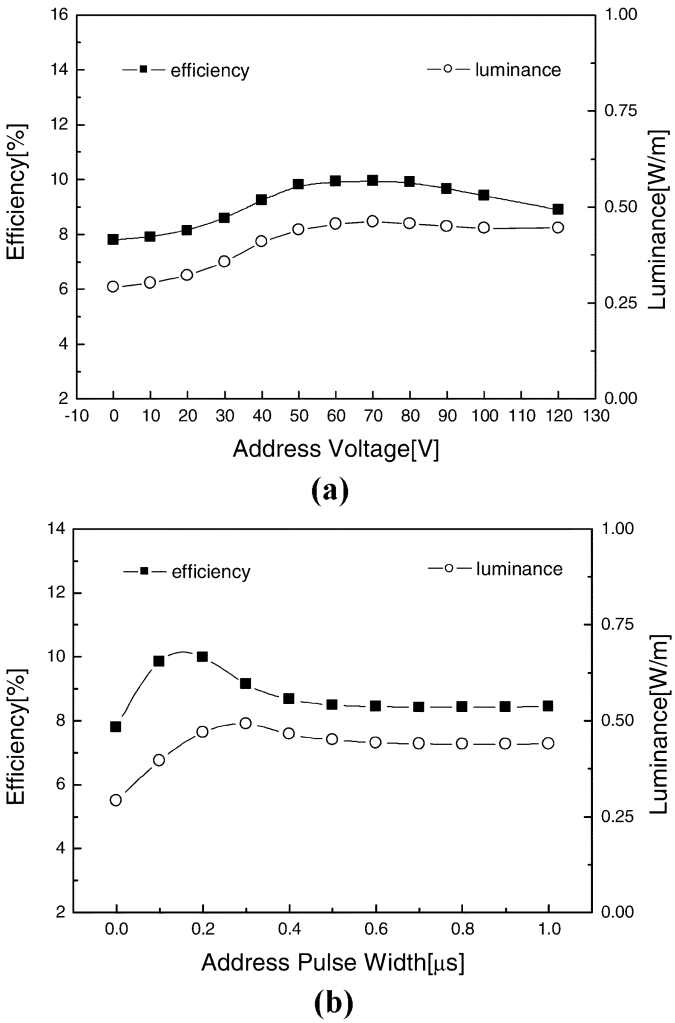

Fig. 13. Variations in luminous efficiency and luminance as function of: (a) voltage (Va) on address electrode address at $Ta = 0.2\ \mu$s and (b) address pulse width (T_a) at $V_a = 70$ V.

high during the sustain discharge, and dropped to 0 V before the off period. When an address bias of 0 V is maintained, many ions are accumulated on the address electrode during the surface discharge. Then, during the off period, a self-erase discharge occurs between the address and the X (or Y) electrode, where the address electrode plays the role of an anode. As the wall charges are erased by the self-erase discharge, the next sustain discharge becomes weak compared with the condition where there is no self-erase discharge.

However, in the case of Fig. 13, the address bias was maintained above 0 V during the discharge current flow, thus a self-erase discharge was avoidable, as fewer ion charges were accumulated on the address electrode. Therefore, as the address bias was increased, the possibility of a self-erase discharge decreased, thereby increasing the luminance.

IV. Conclusion

The microdischarge characteristics induced by a synchronized auxiliary address pulse in an ac-PDP were examined based on a cross-sectional infrared view taken using an ICCD camera. The application of an auxiliary address pulse induced a faster discharge initiation and extended the infrared emission region toward the address electrode, thereby enhancing the discharge efficiency. Plus, an address pulse of 90 V with a width of 400 ns produced the highest IR intensity and largest distribution area toward the address electrode. A further numerical analysis also showed that adopting a synchronized auxiliary address pulse improved the luminance and luminous efficiency due to abundant space charges that lengthened the discharge path, and in turn intensified the surface discharge. Therefore, igniting the predischarge was found to be important for supplying priming particles to the main surface discharge. In addition, the results showed that when T_a was shorter than T_{CFA}, the ion wall charges erased from the address electrode were restored during the surface discharge and a successive face discharge occurred at the next pulse. However, when T_a was larger than T_{CFA}, the ion wall charges were not restored.

References

[1] S.-H. Jang, K.-D. Cho, H.-S. Tae, K. C. Choi, and S.-H. Lee, "Improvement of luminance and luminous efficiency using address voltage pulse during sustain-period of AC-PDP," *IEEE Trans. Electron Devices*, vol. 48, pp. 1903–1910, 2001.

[2] K.-D. Cho, H.-S. Tae, and S.-I. Chien, "Improvement of color temperature using independent control of red, green, blue luminance in AC plasma display panel," *IEEE Trans. Electron Devices*, vol. 50, no. 2, pp. 359–365, Feb. 2003.

[3] J. C. Ahn, Y. Shintani, K. Tachibana, T. Sakai, and N. kosugi, "Effects of pulsed potential on address electrode in a surface-discharge alternating-current plasma display panel," *Appl. Phys. Lett.*, vol. 82, no. 22, pp. 3844–3846, 2003.

[4] Y. Shintani, J. C. Ahn, K. Tachibana, T. Sakai, and N. Kosugi, "Diagnostics and control of three-dimensional behaviors of microdischarge in a unit cell of an AC-type plasma display panel," *J. Phys. D, Appl. Phys.*, vol. 36, pp. 2928–2939, 2003.

[5] Y. Shintani, J. C. Ahn, K. Tachbana, and T. Sakai, "Effects of bias potential on address electrode and driving pulse width to sustain discharge characteristics of an AC-PDP," in *Proc. 9th Int. Display Workshop*, 2002, pp. 817–820.

[6] J. H. Seo, W. J. Chung, C. K. Yoon, J. K. Kim, and K. W. Whang, "Two-dimensional modeling of a surface type alternating current plasma display panel cell: Discharge dynamics and address voltage effects," *IEEE Trans. Plasma Sci.*, vol. 29, no. 5, pp. 824–831, Oct. 2001.

[7] H. C. Kim, M. S. Hur, S. S. Yang, S. W. Shin, and J. K. Lee, "Three dimensional fluid simulation of a plasma display panel cell," *J. Appl. Phys.*, vol. 27, pp. 171–181, 1999.

[8] J. Meunier, P. Belenuer, and J. B. Boeuf, "Numerical model of an AC plasma display panel cell in neon-xenon mixture," *J. Appl. Phys.*, vol. 78, pp. 731–745, 1995.

Heung-Sik Tae (M'00) received the B.S. degree from the Department of Electrical Engineering, in 1986, and the M.S. and Ph.D. degrees in plasma engineering in 1988 and 1994, respectively, all from Seoul National University, Seoul, Korea.

Since 1995, he has been an Associate Professor with the School of Electronic and Electrical Engineering, Kyungpook National University, Daegu, Korea. His research interests include the optical characterization and driving circuit of plasma display panels, the design of millimeter wave guiding structure, and MEMS or thick-film processing for millimeter wave device.

Dr. Tae is a Member of the Society for Information Display. He has been serving as an editor for the IEEE Transactions on Electron Devices, section on flat panel display, since 2005.

Hyun Ju Seo received the B.S. and M.S. degrees from the Department of Electronic Engineering, Kyungpook National University, Daegu, Korea, in 2000 and 2003, respectively.

Her current research interests include the micro-discharge cell and the driving waveform design of plasma display panels.

Dong-Cheol Jeong graduated from Seoul National University (SNU), Seoul, Korea, in 1992. He received the M.S. degree in plasma engineering from SNU, in 1994, where he is working toward the Ph.D. degree.

He worked as a Research Engineer at PDP division in Samsung, SDI from 1994 to 1999. His research interest is the analysis of wall charge characteristics in an ac PDP cell.

Jeoung Hyun Seo received the B.S. degree from the Department of Electrical Engineering, in 1993, and the M.S. and Ph.D. degrees in plasma engineering, in 1995 and 2000, respectively, all from Seoul National University, Seoul, Korea.

He was with PDP Division of Samsung SDI, Chonan, Korea, from 2000 to 2002, where his work focused on the design of driving pulse in ac PDP. Since September 1, 2002, he has been a Professor in the Department of Electronics Engineering, University of Incheon, Incheon, Korea. His research is currently focused on the high-efficiency PDP cell structure, driving method, and numerical modeling in PDP.

Dr. Seo is a Member of Society for Information Display and the Korean Information Display Society.

Hyun Kim received the B.S. and M.S. degrees from the Department of Electrical Engineering, Kyungpook National University, Daegu, Korea, in 1999 and 2002, respectively, where he is currently working toward the Ph.D. degree in electronic engineering.

He is currently with PDP Division of Samsung SDI, Chonan, Korea. His current research interests include the micro-discharge cell and the driving waveform design of plasma display panels.

Mr. Kim is a Member of the Society for Information Display.

Ki-Woong Whang received the B.S. degree from Seoul National University (SNU), Seoul, Korea, in 1972, and the M.S. and Ph.D. degrees in physics from the University of California, Los Angeles (UCLA), in 1976 and 1981, respectively.

He was a Research Engineer in the Plasma Laboratory, UCLA, from 1981 to 1982. From 1982 to 1983, he was with the Plasma Laboratory at the University of Maryland, College Park. In 1983, he returned to Korea, and since then, has been a Professor in the School of Electrical Engineering, SNU.

Dr. Whang is a Member of the American Physics Society, the Electrochemical Society, and the Society for Information Display.